Motion Tracking for Automatically Controlled Functional Electrical Stimulation System in Mirror Therapy Configuration: The Enhanced Lazarus Solution

IEEE Access
Multidisciplinary | Rapid Review | Open Access Journal

Received 4 July 2025, accepted 9 August 2025, date of publication 19 August 2025, date of current version 28 August 2025.

*Digital Object Identifier 10.1109/ACCESS.2025.3600583*

RESEARCH ARTICLE

# Motion Tracking for Automatically Controlled Functional Electrical Stimulation System in Mirror Therapy Configuration: The Enhanced Lazarus Solution

**ELISABETTA SPINAZZOLA[1], (Graduate Student Member, IEEE), ANDREA MONGARDI[1], (Member, IEEE), FABIO ROSSI[1], (Member, IEEE), ANDREA PRESTIA[1], (Member, IEEE), SARA BECCHI[1], ROSANNA CAVAZZANA[1], FEDERICA SAVI[1], JACOPO SECCO[1], DANILO DEMARCHI[1], (Senior Member, IEEE), FABIO PARESCHI[1], (Senior Member, IEEE), AND GIANLUCA SETTI[2], (Fellow, IEEE)**

[1]Department of Electronics and Telecommunications, Politecnico di Torino, 10123 Turin, Italy
[2]CEMSE, King Abdullah University of Science and Technology (KAUST), Thuwal 23955, Saudi Arabia

Corresponding author: Elisabetta Spinazzola (elisabetta.spinazzola@polito.it)

This work was supported by the Comitato Bioetico di Ateneo (CBA) of the University of Turin under Grant 445154.

This work involved human subjects or animals in its research. Approval of all ethical and experimental procedures and protocols was granted by the Comitato Bioetico di Ateneo (CBA) of the University of Turin.

**ABSTRACT** In this work, we present the potential application of an automatic control system for adjusting the parameter values of Functional Electrical Stimulation (FES). FES is a key enabling technology in the functional recovery of patients undergoing neuro-muscular rehabilitation. In this application, successful stimulation outcomes depend on the accurate setting of patient-specific parameters – such as pulse width and stimulation frequency – which are typically determined by physiotherapists based on their clinical experience. The proposed system is implemented in a Mirror Therapy setup, where an injured limb is controlled via FES to replicate the movement of a healthy limb – either belonging to the same patient or to a physiotherapist. The FES activation signal is derived from surface Electromyography (sEMG) recordings of the healthy limb and transmitted to the FES unit after compression using an Average Threshold Crossing (ATC) algorithm. Optimal FES parameters are adjusted through a closed-loop feedback system based on motion tracking of the injured limb, which is continuously compared to the movement of the healthy limb. Additionally, we explore the possibility of replacing the ATC algorithm used for compressing the sEMG signal from the healthy limb with a Compressed Sensing-based approach. This alternative would enable full reconstruction of the sEMG signal–unlike ATC–at the cost of only a minimal increase in computational effort. A prototype was tested on 22 healthy subjects under five different parameter configurations, confirming the feasibility and adaptability of the proposed system.

**INDEX TERMS** Functional electrical stimulation, motion tracking, surface electromyography, mirror therapy, stroke, neuro-muscular rehabilitation, compressed sensing.

## I. INTRODUCTION

Stroke is the third leading cause of years of life lost (YLL) worldwide: age-standardized YLL increased by 12.9% (10.6-15.2) from 1990 to 2007 and by 12.1% (9.9-14.1) from 2007 to 2017. In the post-stroke acute phase, approximately 60-80% of survivors have upper or lower limb motor impairments [1]. Around 40% of people with an acute right hemispheric stroke and 20% with a left hemispheric stroke will present hemiplegia, with upper limbs usually more

The associate editor coordinating the review of this manuscript and approving it for publication was Mehrdad Saif.

affected than the lower ones [2]. While paralysis of the lower limb reduces mobility, paralysis of the upper limbs, on the other hand, reduces human self-care skills [3]. Hemiplegia is characterized by paralysis on one side of the body, typically affecting the muscles of the lower facial region, arm, and leg. In addition to motor problems other lacks may occur, *e.g.* sensation, memory and cognition.

In neuromuscular rehabilitation, restoring voluntary control and functional movement in post-stroke patients remains a significant clinical challenge. Functional Electrical Stimulation (FES) directly activates peripheral nerves to evoke muscle contractions that mimic physiological movement. By delivering electrical currents, FES selectively recruits motor units activating nerves in paralyzed or paretic muscles [4], enabling repetitive, task-oriented training even in severely with severely impaired patients. Recent studies show that adding FES to rehabilitation enhances recovery after muscle-injury-induced paralysis [5].

Furthermore, it is recognized that motor function can be improved through physical therapy and Mirror Therapy (MT). MT involves placing the affected limb behind a mirror so that the reflection of the healthy limb appears in its place, tricking the brain into perceiving movement and providing positive visual and cognitive feedback [6]. This therapy can also stimulate imagination and aid cognitive recovery. Furthermore, recent studies demonstrated that the introduction of Functional Electrical Stimulation (FES) in rehabilitation therapy enhances recovery for patients with paralyzed muscle injuries [5]. FES is a technique that applies electrical currents to activate nerves innervating extremities affected by paralysis [4].

A combination between FES and MT is widely proposed [7], [8]: Hyun Jin Kim et al. demonstrated that FES with MT during post-stroke rehabilitation can effectively improve motor functions of the upper extremity [7]. Mathieson et al also conducted a study aimed at analyzing the potential efficacy of combining MT and FES therapies for the rehabilitation of the post-stroke upper limb, finding increasing functional improvements with the use of these two combined therapies [8]. In this context, the Lazarus system has been developed as an innovative solution that performs neuro-muscular stimulation through FES, with the added advantage of assisting patients in performing functional rehabilitative exercises [9]. The original Lazarus device extracts surface Electromyography (sEMG) signal from the contralateral healthy limb of the patient or directly from the therapist through surface electrodes. The acquired signal is then hardware-processed through the Average Threshold Crossing (ATC) technique, to produce an Activation Signal (AS) that drives the FES attached to the injured limb, causing it to replicate the movement [10]. FES generates a train of current pulses characterized by a bi-phasic rectangular shape, whose configurable parameters are the pulse amplitude [10], the frequency ($f_s$) and the pulse width ($PW$) while the inter-phase interval is fixed to 100 µs guaranteeing a proper stimuli excitability [11]. While $AS_{ATC}$ signal directly controls the stimulation pulse amplitude, the other stimulation parameters have great impact on the therapy output in terms of comfort felt by the patient during the therapeutic session and the number of recruited muscular fibers. These are left to be dynamically set by the therapist. This process results in high subjectivity in therapy delivery and highlights the need for a data-driven approach to assist the operator in setting the stimulation parameters based on the actual physical characteristics of the subject.

To address this issue, various approaches have been proposed in literatures [12], [13], [14], [15], [16], and [17], which have been deeply investigated in the following Section II. Despite their effectiveness, none of these techniques are suitable for integration into the Lazarus system due to increased consumption from both a practical and energy-saving standpoint, conflicting with the rationale of the system, designed to represent an off-the-shelf solution, easily integrable in specialized care facilities.

Unlike previous works, the proposed system introduces a novel closed-loop control architecture that adaptively modulates both $PW$ and $fs$ stimulation parameters, based solely on the precise and quantitative joint trajectory feedback. This approach minimizes the power constraints required by exoskeleton [12] or sEMG acquisition [13]. This allows for the generation of more physiologically limb movements, spanning the entire elbow flexion-extension arc and corresponding vertical hand displacement, using a lightweight and low-power setup. Furthermore, this design supports seamless deployment in specialized care facilities, addressing practical and clinical constraints unmet by previous studies [16], [17]. This integrated, trajectory-driven control mechanism represents a key innovation, unlocking functionalities that previous methods could not achieve or support. In particular, the assistance and support to the operators is provided both during the stimulation and the acquisition of sEMG signals. The innovation does not only optimize the integration of these processes but also enhance their compatibility with the described system, enabling more efficient, precise, and adaptive control. First, with the integration of a motion tracking system through two combined CMOS cameras, it is possible to evaluate the physiological outcomes of the stimulation by the description of few motion parameters. The extracted quantitative physiological parameters and the feedback to adapt the stimulation settings enable the system to converge on a more effective stimulation patter for each individual patient. This feedback architecture allows for personal and automatic management, empowering adaptive calibration of the FES parameters. This solution overcomes the need to gather objective numerical data from the injured limb, whose sEMG signal can become unreadable due to potential rail-to-rail saturation of the front-end amplifier caused by the FES pulses. In addition, since the sEMG of the healthy limb can not be accurately recorded without

using large amounts of memory, we propose its recovery and reconstruction exploiting Compressed Sensing (CS) technique. The method offers a new tool that can be selected by the operator in the case of ineffective stimulation or incorrect AS extraction. As demonstrated in the results, the CS pipeline returns the original sEMG, from which it is possible to derive an AS comparable to the one generated in hardware by the ATC, to guarantee the correct hardware AS extraction. Although the tool brings a slight increase in computational power, it has the main effect of reducing the amount of data to be transmitted and simultaneously providing operators the physiological aspect with respect to muscle activity used for stimulation and motion mimicking. Finally, a feedback loop was implemented for personal and automatic management, enabling adaptive calibration of the FES parameters.

To sum up, the proposed system contributes the following advancements:

- Closed-loop modulation of stimulation parameters. It introduces a feedback-driven mechanism that allows for adaptively adjustment of both the pulse width ($PW$) and stimulation frequency ($f_s$) based on joint trajectory error, avoiding the high power and complexity of exoskeletons [12] and the continuous sEMG acquisition of prior methods [13]. This integrated, trajectory-driven control mechanism constitutes a key innovation, enabling capabilities that are either impractical or entirely absent in prior art.
- Lightweight and low-power setup. The implemented system enables physiologically relevant and complete limb movements, spanning the entire elbow flexion-extension arc and corresponding vertical hand displacement, using only two CMOS cameras for motion capture. Furthermore, this design supports seamless deployment in specialized care facilities, addressing practical and clinical constraints unmet by previous studies [16], [17].
- Overcomes limitations of sEMG acquisition from the impaired limb. Thanks to the real-time motion tracking module for the movement performance evaluation, it is possible to gather objective and quantitative data overcoming the issue of the rail-to-rail saturation of front-end amplifiers caused by FES when monitoring the muscle activity of the impaired limb through sEMG acquisition.
- Compressed Sensing (CS) for healthy limb sEMG recovery. It allows for sEMG signal reconstruction through CS technique, reducing memory requirements while still yielding an AS comparable to the one generated in hardware by the ATC. Although the tool brings a slight increase in computational power, it has the main effect of reducing the amount of data to be transmitted and simultaneously providing operators the physiological aspect with respect to muscle activity used for stimulation and motion mimicking.

The entire methodology proposed in this paper is been patented [18], introducing a concrete technological advancements in the field of neuromuscular rehabilitation by proving a control strategy for the FES parameters setting. The results will be presented for a tested population of 22 subjects from both a statistical and subjective point of view, demonstrating the validation of the innovative features of the system and its practical application.

The paper is organized as follow: in Section II, previous related works are discussed, outlining their main limitations and the specific contributions introduced by our proposed approach. In Section III, the original Lazarus system design is provided with the presentation of the new methodologies: Automatic FES in feedback control loop and sEMG recovery by CS. Then, the experimental protocol is described in Section IV, as also the data processing methodology. In Section V, results are presented for the sEMG-CS reconstruction and FES control parameters determination. In the end, the conclusion is drawn.

## II. RELATED WORKS

As mentioned in the previous section, in the clinical field of neuromuscular rehabilitation, various approaches have been proposed in literature. Wolf et al. [12] proposed a hybrid FES exoskeleton for the pulse width elbow flexion, where the robotic exoskeletons have large power requirements and complex settings. Zhou et al. [13] proposed time-domain sEMG features to evaluate $PW$ and $f_s$, which force to sEMG acquisition and recording analysis. Zheng-Yang Bi et al. [14], [15], used the same technique in ankle and wrist, that does not allow a complete movement pattern of the limb. For the only $PW$, it was also proposed the evaluation of angular velocity and flexion angle in EMG modeling for the ankle flexion [16], [17]. While these methods demonstrate clinical efficacy, their practical implementation conflicts with the Lazarus system's design principles, particularly regarding energy efficiency and ease of integration in clinical settings. The system prioritizes off-the-shelf deployability, which precludes techniques requiring specialized infrastructure or excessive power consumption.

Overall, the integration of all the described implemented functionalities enables to assist and support the operators both during the stimulation and the acquisition of sEMG signals. The innovation does not only optimize the integration of these processes but also enhance their compatibility with the described system, enabling more efficient, precise, and adaptive control. Our comparison of the highlighted literature approaches and our Enhanced Lazarus solution, across control mechanisms, modulation parameters, tested movements, study populations and therapist-patient involvement, are presented in Table 1, underlining the key advancements introduced by our system.

## III. SYSTEM DESIGN

The state of art Lazarus system architecture consists of multiple sEMG acquisition devices, the control platform (PC)

**TABLE 1. Comparative overview of recent FES control approaches.**

| Ref. | Work | Control Mechanism | Modulation | Tested Movement | Population | Therapist–Patient approach | Comparative Advantages Enabled by Enhanced Lazarus |
|---|---|---|---|---|---|---|---|
| [12] | Wolf *et al.* (2017) | Hybrid FES exoskeleton | Pulse Width | Elbow flexion | 7 Healthy | No | Eliminates heavy, energy-intensive exoskeletons by employing a lightweight dual-camera system for real-time control. |
| [13] | Zhou *et al.* (2017) | Time-domain sEMG features | Pulse Width, $f_s$ | Wrist movements | 6 Healthy | Yes | Delivers true real-time closed-loop adaptation of both PW and $f_s$, instead of relying on continuous EMG acquisition and offline processing. |
| [14] | Bi *et al.* (2019) | Time-domain sEMG features | Pulse Width, $f_s$ | Ankle extension / flexion | 6 Healthy | Yes | Reconstructs and tracks full-limb kinematics (elbow flexion–extension). |
| [15] | Bi *et al.* (2020) | Time-domain sEMG features | Pulse Amplitude | Wrist movements | 2 Healthy | No | Achieves sub-second (<256 ms) feedback latency and validates on 22 subjects, versus 600 ms delay and only two subjects. |
| [16] | Carvalho *et al.* (2021) | Angular velocity/EMG | Pulse Width | Ankle flexion | 10 Healthy; 6 Drop-Foot | No | Eliminates the need for combined EMG and angular-velocity sensors, using only motion tracking for adaptive FES. |
| [17] | Li *et al.* (2020) | Angular velocity/Flexion | Pulse Width | Ankle flexion | 10 Healthy | No | Modulates both pulse width and stimulation frequency ($f_s$), rather than pulse width alone, for finer control. |
| | Enhanced Lazarus | Motion tracking | Pulse Width, $f_s$ | Elbow flexion | 22 Healthy | No | N/A |

and the electrical stimulator with electrodes. These essential blocks are highlighted with light blue (contralateral or healthy limb) and dark blue (affected limb) boxes in Fig. 1. The described configuration is based on previous experiments [9], where the therapist's limb (or the healthy limb of the patient himself, if in MT configuration) performs the movement while wearing the acquisition device. The control platform processes the movement to send to the FES device, while the patient's paralyzed limb wears two surface electrodes for the stimulation. In details:

- **Acquisition device**: it is made up of two parts [10]. The first is the Multiple Analog Front Ends (AFEs), which acquires, but does not record, the sEMG signals. The AFE is composed by the sEMG conditioning circuit, designed for differential signal acquisition and a voltage comparator, which extracts the Threshold Crossing events ($TC_{event}$). To this aim, a threshold level (that may change from subject to subject) for the analog sEMG signal is calibrated during the system set-up. The second part is the Apollo 3 Blue Micro Controller Unit (MCU), which is the digital part for ATC computation and data transmission. This device streams AS values every 130 ms as $T_{window}$ to the control platform client through its Bluetooth Low Energy (BLE) transceiver. The $AS_{ATC}$ is evaluated by counting how many $TC_{event}$ have been generated in an observation window. As mentioned, the ATC is an event-based method, meaning that only the significant events that exceed the threshold are considered. The number of such events are referred as $TC_{event}$. Finally, $AS_{ATC}$ is obtained as:
$$AS_{ATC} = \frac{TC_{event}}{T_{window}}. \quad (1)$$
where $T_{window}$ is the observation window length expressed in seconds.
- **Control platform**: its modular software developed using the Python programming language executed on a PC. It receives $AS_{ATC}$ values from the BLE module and processes them real-time to define stimulation parameters that will be sent to the FES module. The user can actively supervise system functionalities by interacting with a custom Graphical User Interface (GUI).
- **FES**: a commercial electrical stimulator device was used. The symmetrical bi-phasic pulse pattern of stimulation has an intensity proportional to the extracted $AS_{ATC}$ and variable every time new $AS_{ATC}$ values are available. The control of the device is via ScienceMode2 communication protocol, which allows the user to update stimulation parameters manually during ongoing stimulation.

The clinical needs addressed in the current work involve:

1) absence of motion feedback in both short and long-term control of the therapy;
2) impossibility of an automatic control in the whole FES pulse parameters set up, according to the effectiveness of the treatment;
3) lack of an original sEMG signal visualization;

The new Lazarus system design included the introduction of new blocks highlighted in the green boxes in Fig.1. To address the first two points: two CMOS cameras were included in the experimental setup for motion tracking and motion parameters analysis.

In the proposed scenario, MT requires the patient (or therapist) to perform a functional movement, from which the sEMG signals are processed to extract $AS_{ATC}$. The resulting movement is seen on the contralateral stimulated paralyzed limb, where FES is applied.

To address the third point, we propose an integration with CS application for sEMG reconstruction and alternative AS extraction. The system can be used remotely and CS also allows for very low power-consuming transmission without losing data. By obtaining the sEMG reconstruction, the effectiveness of the treatment is also ensured.

### A. AUTOMATIC FES IN FEEDBACK CONTROL LOOP

The FES control was investigated by simulating clinical rehabilitation sessions. In addition to controlling FES pulse amplitude through the ATC, we monitored voluntary movement trajectory to select $PW$ and $f_s$ parameters. The idea is

to perform motion tracking to extract motion parameters that can be evaluated to automatically update the FES parameters through a feedback control loop.

For this purpose, the YOLOv8 Pose by Ultralytics [19] provides an efficient and high-performance approach for the human pose estimation, leveraging the YOLO architecture alongside enhancements for accurate, real-time keypoint detection. The YOLO framework is widely used in various research fields for object detection and segmentation tasks [20], [21]. For the current work, the YOLOv8 Pose was employed. This specific model uses a convolutional neural network (CNN) architecture that processes input images or video frames to detect human poses and motion tracking. In the state of art, the available model [22] has been previously trained on large datasets with labeled human poses to learn to detect various body parts and their relationships. In this case, we used the model pre-trained and validated with the COCO8-pose dataset. The model has been used to make inference on the videos acquired by the two cameras system, at 30 frames per second, on the subject under FES stimulation and then predict the locations of the interested anatomical parts. The identification of the positions of specific points in a video frame, usually referred as key points, is possible in real-time,with processing times in the order of hundreds of milliseconds. Generally, the key points can represent various parts of the subject such as joints in this specific case. The locations of key points are usually represented as a set of 2D [x, y] or 3D [x, y, visible] coordinates. For the proposed application, 2D coordinates were sufficient to detect the necessary physical parameters. The pose keypoint output provides a confidence score for every detected point. Moreover, the selected CNN is well know for the speed, accuracy and scalability which allows an easy integration with the existing device application [23]. From the whole processed joints, the proposed application extracts specific points in relation to wrists, elbow and shoulder. These selections were made to identify specific motion features between the healthy limb and the stimulated one. Fig. 2 shows an example of recognition capabilities of the network.

For the feedback control loop, the extracted motion parameters are the physical features of height of the wrist from the table and angle between wrist, elbow and shoulder. These features are evaluated to compare the motion performance, as also the stimulation effectiveness, between healthy and stimulated limbs during the entire time of the stimulation. For each video frame $t$, the height of the wrist $h_t$ from reference position (the initial wrist position before performing the movement, considered equal to the elbow), is calculated as difference between the y-coordinates of wrist at $t$ frame and y-coordinates of the elbow (which is considered the origin of the reference system, supposed to be stationary during the whole stimulation):

$$h_t = w_{y_t} - e_y, \tag{2}$$

where $w_{y_t}$ is the y-coordinate of the wrist at $t$ frame and $e_y$ is the elbow one. $h_t$ is the scalar value of the height of the wrist from the plain at $t$ frame. Now, we define $\vec{h}$ as $\vec{h} = [h_1, \dots h_t, \dots h_F]$, the union of the heights evaluated during the whole stimulation for each frame, where $F$ is the total number of video frames. In the same way, the angle parameter at $t$ frame was calculated as the angle between two vectors as

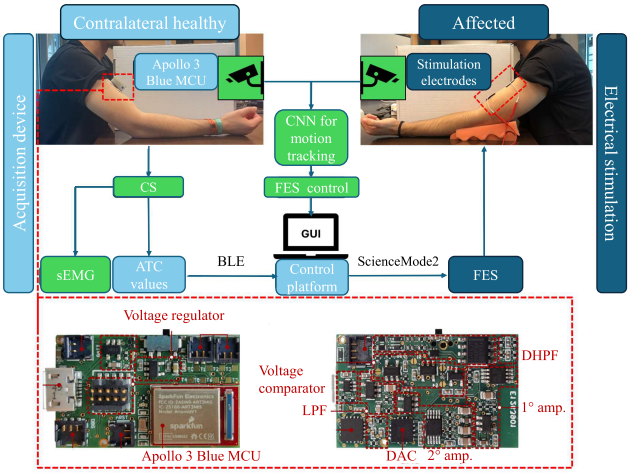


**FIGURE 1.** Lazarus system's blocks where light blue and dark blue boxes highlight the original existing blocks. Starting from the healthy (light blue boxes), ATC values are extracted from sEMG and sent to the control platform, through BLE. The control platform defines FES pulse intensity and allows for manual setting of *PW* and $f_s$. With the ScienceMode2, the stimulation is sent to FES linked to the patient's arm (dark blue boxes). The Printed Circuit Board (PCB) of the acquisition device is shown with its main components. The new enhanced Lazarus system design is highlighted by green boxes. Two cameras are included to record the movement and videos are processed through the CNN. FES control is embedded inside the control platform. On the other hand, from the healthy side, CS framework is applied for sEMG recovering.

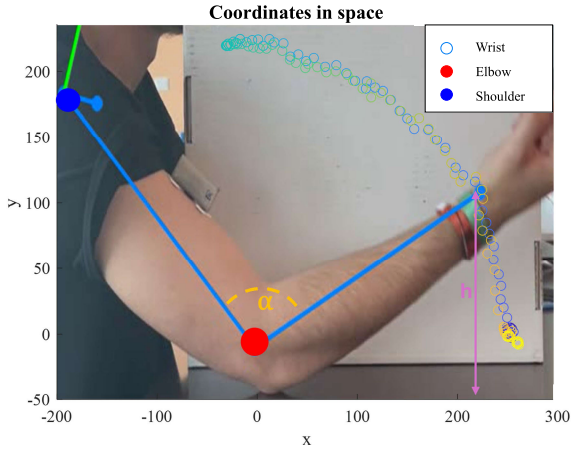


**FIGURE 2.** Set phase coordinates in the space for the wrist, elbow and shoulder of the healthy arm. The shoulder in blue, as the elbow in red, are obtained from the mean of all the frame positions. The wrist coordinates follow the full movement going from blue to yellow. Overlapped to the coordinates, the original video frame is shown, where the full limb is highlighted in blue through the CNN motion tracking markers. The evaluated parameters height and angle are shown as $\alpha$ and $h$.

follows:

$$\vec{p}_t = e_{x,y} - w_{x_t,y_t}, \tag{3}$$

$$\vec{q} = e_{x,y} - s_{x,y}, \tag{4}$$

$$\alpha_t = \cos^{-1}\left(\frac{\vec{p}_t \cdot \vec{q}}{|\vec{p}_t|\,|\vec{q}|}\right), \tag{5}$$

where for each frame $t$, $\vec{p}_t$ is the segment between elbow and wrist, $e_{x,y}$ are the frames averaged elbow coordinates, $w_{x_t,y_t}$ are the wrist coordinates for each frame $t$, $\vec{q}$ is the segment between elbow and shoulder, supposed to be equal between all the frames, $|\vec{p}_t|\,|\vec{q}|$ is the product between the magnitudes of the two vectors, $\vec{p}_t \cdot \vec{q}$ is the scalar product of the two vectors, $s_{x,y}$ are the frames average shoulder coordinates and $\alpha_t$ is the scalar value of the angle between the two segments of the arm at frame $t$. As the height, we define $\vec{\alpha} = [\alpha_1, \ldots \alpha_t, \ldots \alpha_F]$. The elbow and shoulder joints are assumed to remain stationary throughout the movement. This procedure is applied to each limb to evaluate the movements of both the stimulated and the healthy arms. For this purpose, if during the movement repetition the parameters are comparable between the two limbs, $f_s$ and $PW$ setting should be appropriate to perform an efficient stimulation. Otherwise, $f_s$ and $PW$ parameters will be adjusted by the following feedback control loop. Supposing to start an exercise session, exemplified in Fig.3, beginning from the first movement repetition $n = 1$ of the total $N$ repetitions of flex-extension pattern to be performed, $f_s$ and $PW$ will be firstly imposed to the minimal nominal values suggested by the literature and referred as $f_{s_i}$ and $PW_i$ for the first iteration loop $i$. During each repetition, the motion-tracking tool extracts the height vector $\vec{h}$ and the angle vector $\vec{\alpha}$ for both the healthy and the paretic limb. If the maximum extensions of height and angle $h_p$ and $\alpha_p$ achieved by the paralyzed limb are similar to the maximum variables $h_f$ and $\alpha_f$ achieved by the healthy limb, the repetition count is incremented to $n + 1$ with the same $f_{s_i}$ and $PW_i$ values until the end of the exercise. Otherwise, $f_{s_i}$ and $PW_i$ will be incremented of generally, 10 µs for $PW$ and 50 Hz for $f_s$ to the next iteration $i + 1$. The selected increment steps and starting values are based on a trade-off between physiological sensitivity and literature suggestions. In particular the steps size have been shown in prior FES literature to be the minimal change that elicits distinguishable modulation in muscle contraction without excessive jump in perceived discomfort [11].

Moreover, at the current stage of the system development, we decided to implemented these step-wise increments in order to retain a certain control over the stimulation parameters for the subject safeness and to evaluate the efficacy of the stimulation patterns under investigation. In particular, the fixed-increment strategy we adopted represents a compromise between improving the effectiveness of stimulation control and minimizing patient fatigue to multiple stimulations. A simpler approach, such as the proposed one, ensures fewer stimulations and less time to achieve the convergence of efficient FES parameters.

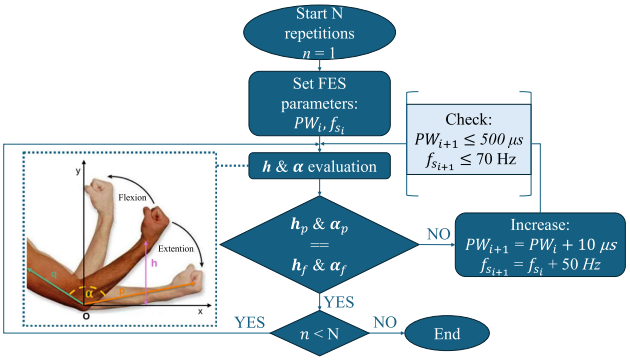


**FIGURE 3.** FES system feedback control loop sets $PW$ and $f_s$ through height $h$ and angle $\alpha$ comparison between healthy and paralyzed limb at each $n \leq N$ iteration (movement repetition). $h_p$ and $\alpha_p$ are referred to the paralyzed limb, while $h_f$ and $\alpha_f$ to the healthy one. On the left, a visual representation of height and angle variables is shown. The reference system is set with the elbow as reference origin.

In addition to the height and angle of the movement, the wrist instantaneous velocity is evaluated to have a referenced value regarding the motion. The velocity at $t$ frame $v_t$ is calculated as the ratio between the Euclidean distance $d_t$ performed by the wrist between the frame $t$ and $t + 1$ and the corresponding frame duration $T$ evaluated in seconds.

$$d_t = \sqrt{(w_{x_{t+1}} - w_{x_t})^2 + (w_{y_{t+1}} - w_{y_t})^2}, \tag{6}$$

$$v_t = \frac{d_t}{T}, \tag{7}$$

where the frame period $T = s/F$ is expressed as ratio between the whole video duration $s$ and the total number of video frames $F$. We define the height vector as $\vec{v} = [v_1, \ldots v_t, \ldots v_{F-1}]$.

### B. SEMG RECOVERY AND ATC CALIBRATION FROM CS

CS technique is applied to a discrete-time representations of the acquired signal. The input signal is first split into windows of $n$ consecutive samples taken at the Nyquist frequency $f_{Ny}$, and CS is applied to each windows separately. CS theory is based on the sparsity property of the signal: instances $x$ of the input signal can always be represented as a linear combination of a few vectors (down to $\kappa \ll n$) of a proper sparsity basis $\Psi \in \mathbb{R}^{n \times n}$. Mathematically, $x = \Psi\xi$, where $\xi \in \mathbb{R}^n$ is a coefficients vector with at most $\kappa$ non-zero elements, i.e., $\|\xi\|_0 \leq \kappa$, where $\|\cdot\|_0$ stands for standard $\ell_0$ norm. In this case we say that the signal is $\kappa$-sparse.

The CS exploits the sparsity property to acquire a signal with a number of samples $m$ that is lower with respect to what expected by Nyquist's law requires, i.e., lower than $n$, with a compression ratio defined as $CR = m/n$. The $m$ samples are computed as the projections of $x$ on a set of $m$ sensing sequences, arranged as the rows of the sensing matrix $A \in \mathbb{R}^{m \times n}$. Measurements are generally arranged in a vector $y \in \mathbb{R}^m$, computed as $Ax = A\Psi\xi$. Under some constraints [24], [25] on $\kappa$, $m$ and $n$ (in details, $m$ has to be larger than a threshold value that depends on $\kappa$

and $n$) and on the sensing matrix $A$ (the so called Restricted Isometry Property (RIP) [25], that can be simply satisfied by randomly generating its rows [26]), theoretical results state that the reconstruction of the input signal can be simply achieved by looking for the sparsest signal that is compatible with the achieved measurement vector. In practical cases, the reconstructed signal $\hat{x} = \Psi\hat{\xi}$ is obtained by solving the convex optimization problem:

$$\begin{aligned} \min_{\hat{\xi}} \quad & \|\hat{\xi}\|_1 \\ \text{s.t.} \quad & \|A\Psi\hat{\xi} - y\|_2 \leq \varepsilon \end{aligned} \tag{8}$$

where the more practical $\ell_1$ norm is used instead of the computationally-complex $\ell_0$ norm, and $\varepsilon$ is used to take into account the effect of noise.

CS has already been successfully applied to sEMG signals [27], [28]. In this work, we allow the operator to select the usage of CS to enable the recovery of sEMG when necessary, as a new simple, effective, and hardware-friendly compression technique useful to minimize data transfer requirements. Indeed, in the current version of the Lazarus device, only the count of the number of times the signal exceeds the threshold is returned through an hardware timer [10]. In this configuration, sEMG information along the full movement is lost and the physician has not the possibility to refer to the original signal. On the other hand, there is often the need to visualize the original sEMG to check if the signal sent to the diseased limb is adequate to stimulate it. There may be cases where the original movement is abnormal or incorrect and, consequently, the generated stimulation is not functional to perform the movement. The proposed application, instead of capturing only the threshold crossing events, adds the sEMG signal acquisition with the CS framework. This gives the advantage of a fully sEMG recovering and simultaneously obtaining an AS comparable to the one obtained by the ATC. The ATC method initially involves comparing amplified and filtered sEMG signals against a certain threshold that is obtained through the calibration process. For this reason, this method is defined as event-based meaning that only the significant events that exceed the threshold are considered. In this view, having double ASs extracted from two parallel procedures, enables the correct assessment of the ATC threshold calibration and the effective AS elaboration.

From an implementation standpoint, CS encoding (i.e., the generation of the vector $y$) used a simple algorithm implemented in 8-bit Micro controller such as the Apollo 3 Blue employed the acquisition device. Furthermore, using an antipodal random sensing matrix $A \in \{-1, 1\}^{m\times n}$ further decreases the required hardware complexity, removing the need of an hardware multiplier with no penalties in terms of signal reconstruction [29]. Reconstruction is instead achieved on the control platform, where a much higher computational power is available. The chosen optimization algorithm is the Basis Pursuit De-noising (BPDN) adopting the SPGL1 algorithm. The applied sparsifying matrix is in Discrete Wavelet Transform domain, Symlet 6.0 mother wavelet, in 64 × 64, 128 × 128, 256 × 256, 512 × 512 dimensions of the windows.

### C. GUI AND USABILITY

The graphical user interface (GUI) was developed using Python, employing *Tkinter* for the initial setup phase and *OpenCV* for calibration and rehabilitation phases. The GUI comprises four main steps: selecting webcams and entering patient data, setting parameters, calibration, and managing rehabilitation sessions. Brief explanatory pop-ups are displayed before each interface to ensure usability. Certain interface keywords are intentionally presented in Italian, as the system is primarily intended for Italian rehabilitation centers. The initial interface, as shown in Fig.4a), assigns webcams to the right or left arm (left window) and collects patient information, including the social security number and the number of planned repetitions for the session (right window). In the calibration phase, real-time measurements of the patient's arm height and angle are displayed, enhancing accuracy. The corresponding metrics, presented in degrees for angles and centimeters for height, are more intuitive and reliable for the user compared to pixel-based measurement. The conversion of height is performed by multiplying the height value, in pixels, by a specific scale factor, $k_{cm}$:

$$k_{cm} = \frac{(l_m * 100)}{l_p} \tag{9}$$

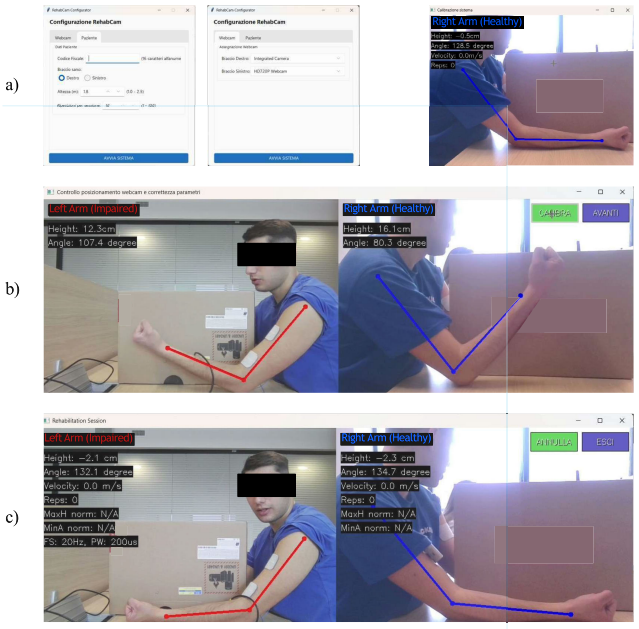


**FIGURE 4. GUI implementation and interfaces for the system setup: a) Selecting webcams, entering patient data and starting the calibration phase are presented as pop-up dialogs to guide the user through the setup process, b) Calibration of system parameters: the interface displays height and angle of the movement in centimeters and degree, respectively, c) Rehabilitation session: the interface displays movement performance metrics, the number of repetitions completed and the current stimulation parameters.**

where $l_m$ represents the anthropometrically estimated forearm length, multiplied by 100 to convert it into centimeters, calculated by multiplying the patient's height by an anthropometric factor [30], and $l_p$ is the pixel distance from elbow to wrist, calculated as the Euclidean distance between the elbow and the wrist. The interface allows for recalibration of the pixel-to-centimeter conversion factor for each arm if necessary, as illustrated in Fig.4b). During calibration, the system focuses exclusively on the healthy arm to determine minimum and maximum movement values, which is essential for min-max scaling of height and angle measurements in subsequent phases. After calibration, the system automatically transitions to the rehabilitation session, depicted in Fig.4c). The system setup interface takes about 30 seconds, parameter calibration approximately 40 seconds, and the calibration phase about 5 seconds, keeping the total setup time under two minutes, indicating high usability.

In the rehabilitation session interface, real-time data such as height, angle, velocity, completed repetitions, normalized movement metrics, and the configuration of fs and PW currently in use by the operator are displayed for both arms. The user retains the ability to interact with the interface, such as deleting parameter updates when incorrect movements result from low ATC values, causing insufficient stimulation intensity. If the measured values for the impaired arm deviate from predefined tolerance ranges, the system automatically adjusts the stimulation parameters and alerts the operator via a pop-up message. Otherwise, the repetition counter is updated upon successful movement. If the patient reports fatigue or discomfort, the session can be immediately interrupted using an emergency button. The GUI design adheres to usability standards defined by IEC 60601-1-6 and IEC 62366, aligning with European Medical Device Regulation 2017/745 (MDR).

## IV. EXPERIMENTAL PROTOCOL

The experimental protocol, reported with the code 445154, named "Event based system validation for the Functional Electrical Stimulation (FES)" has been presented to and approved by the Comitato Bioetico di Ateneo of the University of Turin. All the the subjects enrolled for this study were asked to sign an informed consent that has been approved by the same ethical committee during the protocol's assessment.

The aim was to obtain a proof of concept regarding the automatic control of the electrical stimulation pulse parameters. A total of 22 healthy subjects were involved aiming to construct a statistically relevant sample which could satisfy the imposed inclusion criteria: age $>$ 18 years, absence of active implantable devices and sign the informed consent. The experimented test sessions are made up of 5 combinations of $PW$ and $f_s$ values, chosen to cover the majority of possible cases based on state of the art standards [11]: $f_s$ from 10 to 70 Hz and $PW$ from 20 to 500 µs. The 5 combinations are described as follows:

1) $f_s$ = 35 Hz; $PW$ = 300 µs, considered most physiological;
2) $f_s$ = 20 Hz; $PW$ = 300 µs, which combines low $f_s$ and medium$PW$;
3) $f_s$ = 20 Hz; $PW$ = 450 µs, which combines low $f_s$ and high$PW$;
4) $f_s$ = 70 Hz; $PW$ = 150 µs, which combines high $f_s$ and low$PW$;
5) $f_s$ = 70 Hz; $PW$ = 300 µs, which combines high $f_s$ and medium$PW$.

These configurations and each subject's movement performance data served as the basis for parallel, real-time evaluation of the feedback control loop and, consequently, for determining the system's optimal stimulation settings based on height and angle parameters. The patient's motion throughput (in terms of $h$ and $\alpha$) was used as input to the feedback loop in order to retain control over the stimulation and assess its ability to converge toward the optimal stimulation configuration for each specific patient. The subjects were asked to perform an elbow flex-extension movement of both upper limbs. This movement was chosen due to its importance in subsequent rehabilitation phases, which focus on recovering functional movements essential for daily activities. As the basis for reach-and-grasp activities [31], this single-joint motion precedes more advanced, multi-joint coordination exercises in subsequent therapy sessions. The current study was therefore limited to a single-joint, as part of a proof-of-concept implementation based on a mirror therapy setup, which is widely adopted in early-stage post-stroke rehabilitation [32], [33]. This approach was chosen based on clinical feedback suggested by physiotherapists, as it allows for simpler control, better user monitoring, and more reliable evaluation of the core components of the closed-loop system.

The subjects were seated with their forearms in supine position and elbows leaning on the table, while their body movements were captured using two cameras, one pointed towards the healthy arm and the other towards the stimulated one. The sampling frequency of cameras was set to 30 fps, which has proven to be enough to achieve accurately human joint flexions and extensions positions. All key points of the joints of our interest were recognized correctly by the CNN.

The coordinates were processed in 2D points configuration inside the reference system, with the elbow as origin. Before proceeding to test phase, two preliminary steps was conducted. Firstly, a set up phase was performed and the complete movement for each arm was recorded once to normalize test sessions movements (in terms of spatial coordinates). Then a signal calibration was carried out. The healthy arm performed flex-extension movements using voluntary exciting force in order to generate an $AS_{ATC}$ signal used to set stimulation intensity. $AS_{ATC}$ was then modulated based on the contralateral arm stimulation pulses of increasing amplitude until the stimulated limb reached the desired movement, as shown in Fig. 5. The figure shows

the increase in current intensity and the resulting height and angle measurements during movement repetitions. As the stimulation intensity increases, both the peak height and angle change progressively until the full range of motion is achieved. At this stage, it is essential to verify that the increase in pulse intensity does not cause discomfort or pain for the subject. This calibration step aims to determine the ATC threshold during muscle rest and the maximum variation of ATC value during subsequent movement repetitions, as described in [9].

The electrodes used in this experiment were the same as those utilized in a previous work [9]. For sEMG detection, Kendall$^{TM}$ H124SG (Ag/AgCl,24 mm) pre-gelled electrodes were used, placing them in the center of the biceps muscular body. Then two electrodes HASOMED® RehaTrode (5 cm×9 cm) were placed, above and below the biceps. In this phase, skin preparation was important, applying a conductive gel on electrodes surface to enhance adhesion to the skin and avoid misplacement.

A test session was carried out for each of the 5 planned configurations. During each test the subject had to perform the same movement for 20-40 s, making at least 5 repetitions in order to evaluate the repeatability and the stimulation effect.

We also examined the potential effects of stimulation-induced fatigue by conducting an additional, dedicated fatigue test. The configuration from test session 1 was employed, performing 20 repetitions of the movement with a constant stimulation intensity based on $AS_{ATC}$ extracted from the subject's initial motor act.

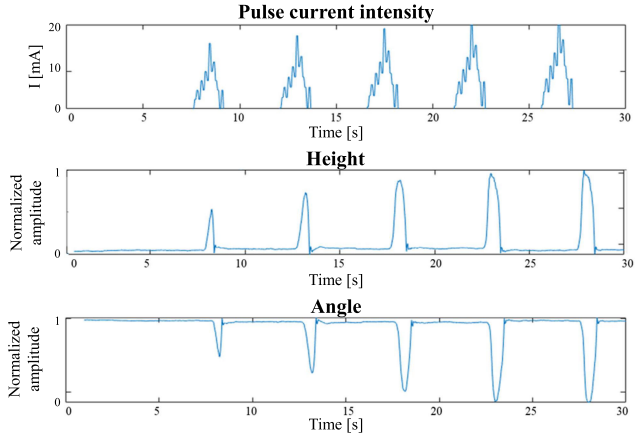


**FIGURE 5. Stimulated arm calibration. By delivering progressively larger current pulses (top), the resulting peak movement height (middle) and peak movement angle (bottom) both increase under ATC modulation. All amplitudes have been normalized with respect to the set phase parameters.**

It should be noted that the selected movement for all tests is based on the contraction force of the healthy arm, which varies with each repetition. The actual muscle force generated and delivered to the stimulated limb was taken into account via $AS_{ATC}$ recording, subsequently used for the comparison between the movements of the two limbs.

### A. SURVEY

To strengthen the proof of concept validation and enhance statistical robustness, each subject completed a survey about their sensations during each test session. In particular, they rated the following variables related to the execution of the movement during stimulation on a scale ranging from 1 to 5 (1 = minimal, 5 = maximal):

1) Intensity: level of stimulation power felt. This variable should be consistent with the efficacy of test session;
2) Pain: degree of pain felt. Used to verify that the stimulation does not cause physical hurt;
3) Fatigue: amount of effort perceived. If Fatigue is low and Intensity is high, the stimulation should be effective;
4) Easiness: subjective rating of movement fluidity and agility. If the stimulation is effective, Easiness should be high;
5) Annoyance: level of discomfort or annoyance experienced. Control parameter to verify that the stimulation does not hurt the patient.

For fatigue test, subjects were asked an additional question about when they first begin to feel fatigue during the session, rated from 1 at the start to 5 at the end. The survey helped verify consistency with quantitative data on the correlation between movements of healthy and stimulated limbs.

### B. DATA ANALYSIS

Data gathered from the experiment was analyzed in two steps. In the first part, sEMG and AS envelope reconstruction was achieved though the CS framework, comparing the obtained AS with the one achieved by ATC. The dataset included different type of sEMG signals recorded at a sampling frequency of 1000 Hz from different muscles: Biceps Brachii, Flexor Carpi Ulnaris, Lateral Deltoid and Extensor Carpi Ulnaris. For the first three muscles, an elbow flex-extension was performed, while for the Extensor Carpi Ulnaris a wrist flex-extension was done. In the second part, control of the proposed FES system was tested on 22 recruited subjects. All the data were preprocessed and normalized. The normalization was performed on the height $\vec{h}$, velocity $\vec{v}$ and angle $\vec{\alpha}$, evaluated on the wrist during the test phases, across the same features evaluated during the set up phase, as described in Section IV, under normal conditions for both healthy and stimulated arms. For the height case, $\vec{h}_{\text{norm}} = \vec{h}_{test}/\vec{h}_{set}$. The parameters are then normalized in a range from 0 to 1. All the reported variables results are expressed in normalized amplitudes.

### C. PERFORMANCE METRICS

To evaluate the implemented system, we used the Correlation Coefficient (CoC) metric to:

- Compare the novel $AS$ signal obtained via CS against the $AS_{ATC}$ signal produced by the traditional method.
- Quantify the syncronization between healthy and paralyzed limb movements during the test sessions.

This metric values typically ranges from −1 to 1, where 1 represents a perfect alignment of the two signals.

Regarding the evaluation of the *AS* signal obtained via CS method, the metric was calculated between the standard $AS_{ATC}$ and the *AS* signals for all the CS tests using different window sizes $n = 512, 256, 128, 64$ and $CR = 1, 2, \ldots, 6$.

On the other hand, to perform a comparison between the two movement and quantify their correlation, the CoC was calculated on the time-series signals of movement height and angle for both the arms across all the conducted tests. For a given test session, we compute the CoC by comparing the height vectors of the healthy and paralyzed limbs as follows:

$$\mathrm{CoC}_h = \frac{\sigma_{\vec{h_p}\vec{h_f}}}{\sigma_{\vec{h_p}}\sigma_{\vec{h_f}}} \tag{10}$$

where $\sigma_{\vec{h_f}}$, $\sigma_{\vec{h_p}}$ and $\sigma_{\vec{h_p}\vec{h_f}}$ are the standard deviation of the healthy arm height values, the standard deviation of the stimulated one and the covariance of both, respectively. Since the stimulated limb's response is inherently delayed relative to the healthy limb, for the current analysis we also computed the Cross-correlation metric. By focusing on the maximum Cross-correlation value for each signal pair, this metric captures the true similarity between the two movement profiles while automatically compensating for any latency. For discrete functions, Cross-correlation is defined as:

$$(f \star g)[n] = \sum_{m=-\infty}^{\infty} \overline{f[m]} g[m+n], \tag{11}$$

where $n$ is the latency and $m$ is the sample.

We further supported our evaluation by incorporating participants' survey responses. This allowed us to assess whether each individual's subjective perception of the stimulated limb's movement quality aligned with the objective similarity measures (CoC and Cross-correlation).

Finally, we assessed the impact of muscle fatigue on movement performance. This metric specifically allows to distinguish between suboptimal exercise execution caused by ineffective stimulation patterns and the decline in contraction capacity which occurs over time with prolonged muscle stimulation. Fatigue was measured as percentage decrease between two consecutive peaks, for both height and angle.

$$dec_{\%} = \frac{(pk_{\mathrm{i}}) - (pk_{\mathrm{f}})}{(pk_{\mathrm{i}})} * 100 \tag{12}$$

Moreover, this metric enables identification of the optimal number of repetitions for a given exercise, beyond which the stimulation pattern loses efficacy and no additional therapeutic benefit is achieved.

These evaluation parameters were chosen to comprehensively assess both stimulation efficacy and movement performance by directly correlating the angle and height parameters over time between healthy and paralyzed arms. These parameters provide immediate information about the movement trajectory, since the analyzed motion occurs symmetrically in a single plane, namely the sagittal plane. Moreover, the evaluated metrics indirectly allow for assessment of the stimulation's energetic efficiency, which is subject-specific, as it depends on each individual's physiological characteristics. This aspect can be measured both via the survey and by the movement performance tracked with motion-tracking technology.

These metrics were selected to cover all of these aspects without requiring analysis of muscle-contraction patterns, because the sEMG signal recorded from the stimulated arm would be completely obscured by the electrical stimulation itself, rendering such an analysis inconclusive.

## V. RESULTS AND DISCUSSION

Results are reported in order to evaluate the reliability of the proposed system. The experimental analysis consists of 3 sections: the sEMG reconstruction using CS technique and AS comparison, the FES loop control system for setting stimulation parameters and a brief assessment on the FES impact on muscle fatigue.

### A. SEMG IN CS RECONSTRUCTION AND AS COMPARISON

All results are associated to the possible combination of configurations given by the following parameters: windows size $n = 512, 256, 128, 64$, $CR = 1, 2, \ldots, 6$. Here, Biceps Brachii and Extensor Carpo Ulnaris sEMG and the respective $AS_{ATC}$ results are shown. Fig. 6 demonstrates successful of achieving the sEMG reconstruction with a good CS, where Fig. 6a is the original sEMG and Fig. 6b is the recovered sEMG, up to CR = 6. The reconstructed signal achieved a correlation coefficient (CoC) of 0.91 with the original sEMG. Moreover, it can be noted that CS inherently denoises the signal, which is advantageous for EMG processing.

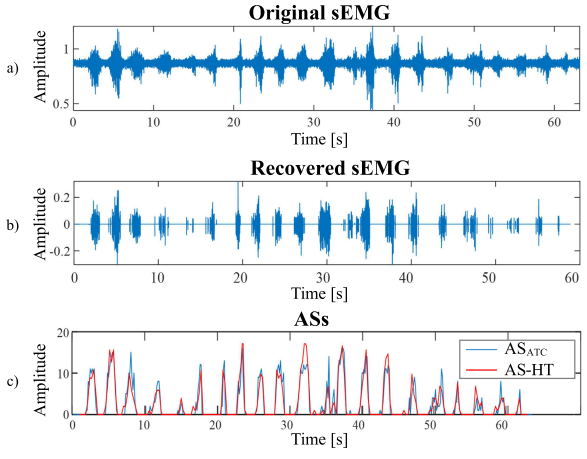


**FIGURE 6.** a) A time domain waveform of the original Extensor Carpo Ulnaris sEMG. b) Reconstruction of the sEMG signal via Compressed Sensing (CS). c) Overlaid comparison of the original $AS_{ATC}$ (blue) with the one obtained applying the Hilbert Transform (HT) to the reconstructed sEMG signal (red). The results are shown for a window length n = 256 and Compression Ratio (CR) = 6.

In Fig. 6c, the AS comparison is shown. The original AS in blue performed by ATC, is reliably obtained also from the Hilbert transform evaluated on the reconstructed sEMG.

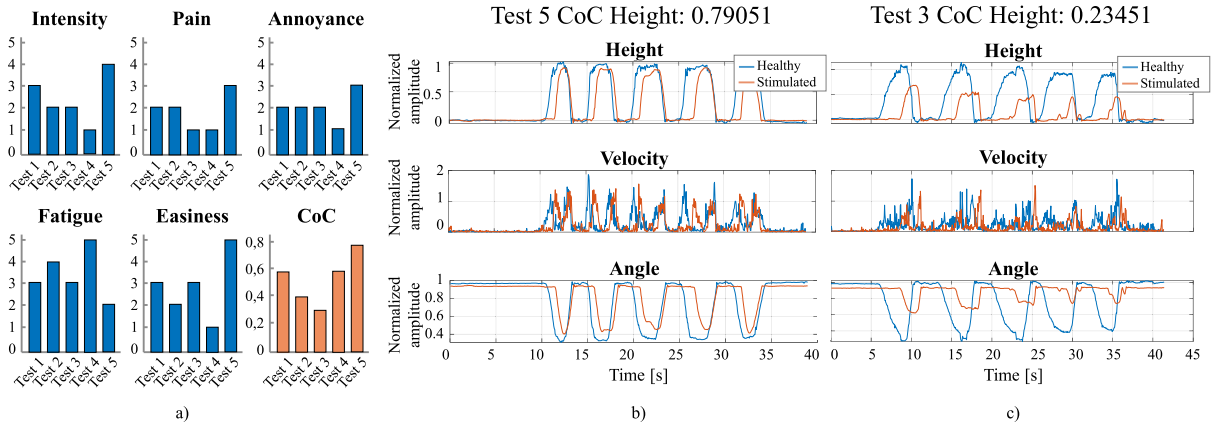


**FIGURE 7.** Example outputs from a subject's stimulation session: a) Survey responses given by the participant with respect to the perceived sensation reported for each test conducted (blue) and Coefficient of Correlation (CoC) values calculated on the movement profiles of healthy and paralyzed arms (orange). b) Time-series profiles of healthy (blue) versus paralyzed (red) arm movements during test session 5. c) Time-series profiles of healthy (blue) and paralyzed (red) arm movements during test session 3, resulting in a reduced Coefficient of Correlation (CoC) between the two movement profiles.

The close correspondence holds up to a compression ratio of 6 ($(CR = 6)$, confirming reliable AS recovery from the CS-reconstructed signal. Across all tested sessions, the CoC values between the two types of AS signals were always at least greater than 0.9 and never less than 0.85. The highest correlations occurred with window lengths of 256 and 512 samples. Overall, AS obtained from the reconstructed sEMG did not show any differences with the standard one ($AS_{ATC}$).

The possibility of retrieving the original is important for a twofold reason. Whereas the most important aspect is clearly allowing the medical team to check the sEMG signal in case of need, there are also a few technical issues that may be solved by the availability of the original sEMG signal. As discussed in detail in the next section, there may be instances where the healthy limb's movement and $AS_{ATC}$ intensity appear adequate, yet the stimulated limb still fails to perform the movement correctly. This may also be due to issues that occur during the movement of the stimulated limb, which cannot be detected without access to the original sEMG.

As an example, emblematic cases exist in which the first contraction leads to a lower paralyzed arm movement due to a slight intensity of the $AS_{ATC}$ for low stimulation contraction, while during the second repetition, a normal AS intensity reveals an almost nonexistent stimulated arm response. This is the typical scenario in which the operator does not know if the $AS_{ATC}$ has been correctly evaluated or the original sEMG signal was too weak. It is worth recalling that the $AS_{ATC}$ is evaluated through the use of a threshold applied on the sEMG signals. Such a threshold is determined during the calibration phase, make it working for the specific patient. In the actual device status, a potential error made on the AS evaluation (e.g., for a wrong threshold) can not be identified, since the absence of the sEMG signals. Even in this case, we were not able to discriminate the cause, since the CS framework has been applied offline respect to the stimulation phase. For this reason, the main clinical advantage brought by the proposed work, can lead to a technical benefit, which overcomes the actual limit of calibration phase. In the actual Lazarus system, the calibration phase is fundamental for the threshold identification to apply on the AS extraction. It is based on the activation profile which makes the framework patient-specific. With the proposed algorithm, threshold tuning becomes unnecessary, as the activation signal is extracted directly from the reconstructed sEMG. The implemented CS framework, which allows for direct reconstruction of sEMG signals, therefore unlocks a spectrum of alternative solutions, enabling the $AS_{ATC}$ features to be replaced with more precise and varied sEMG-envelope representations. In this case, in Fig. 6c the Hilbert Transform has been computed on the recovered sEMG obtaining the envelope of the signal. Such method is one of the possible way to achieve the same information content as the $AS_{ATC}$ without a threshold dependency.

In terms of complexity with respect to the original Lazarus device, the CS framework certainly requires an additional processing block and higher transmission capability. Indeed, we may recall that in the original device, the $AS_{ATC}$ value is transmitted every 130 ms [10], leading to about 8 samples per second. With the proposed CS-based approach, using a 1000 Hz sampling rate and CR $=$ 6, which has been shown to enable high-quality reconstruction, the transmission protocol delivers 166 samples samples per second (about 22 samples every 130 ms). This data rate does not sound excessive considering the overhead of the BLE protocol. Although our current study applies CS-based reconstruction offline, evaluating its real-time feasibility is essential for practical deployment. Considering the literature, [34] analyses a CS system for ECG signals, and include some measurement for the decoding performance when the decoding algorithms is OMP running an a low-energy ARM Cortex M7 microprocessor. With $n = 256$, $m =$

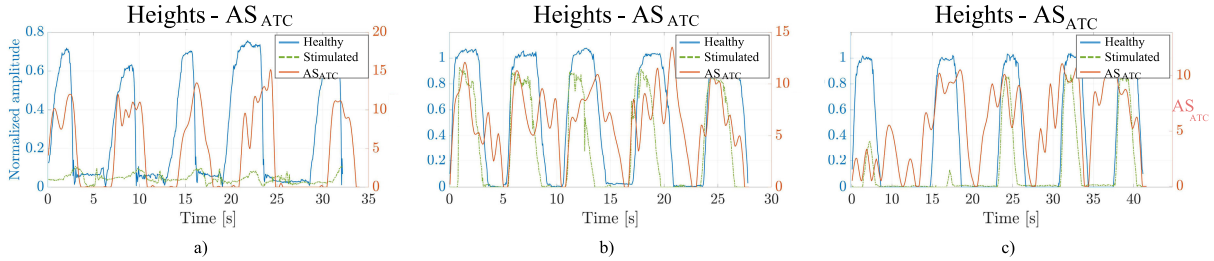


**FIGURE 8.** Time-series comparison of healthy (blue) versus paralyzed (green) arm height under the same $AS_{ATC}$ pulse stimulation intensity (red) derived from the healthy limb. a) Example of an inefficient FES parameters pattern: normal $AS_{ATC}$ intensity and correct movement of the healthy arm, while the stimulated arm exhibits only a weak response. b) Example of an efficient FES parameters pattern: with normal $AS_{ATC}$ intensity, the paralyzed arm produces a proper movement trajectory. c) Example of variable response across repetitions: during the first repetition a minimal paralyzed arm movement, due to an initially low $AS_{ATC}$ intensity, is shown. The second repetition shows a normal $AS_{ATC}$ intensity but the stimulated arm's response remains almost nonexistent. This pattern indicates that achieving an adequate output in the stimulated limb depends not only on the correct $AS_{ATC}$ stimulus intensity (first repetition) but also on the subject's sensory feedback and cognitive understanding the desired movement (second repetition).

68 (*CR*: 1:3.7) samples and sample frequency of 360 Hz, authors observe a decoding times in the order of 711 ms. In our case, considering $n = 256$ and $m = 68$ in the example, but a sampled frequency of 1 kHz, 256 ms (instead of the observed 711 ms) would be necessary for a real-time decoding. Indeed, considering: *i)* the higher *CR* (1:6) achievable by our system; *ii)* although the real-time decoding performance demonstrated in [34] meets the requirements for our proposed system, the decoding speed we measured here, while close, still falls slightly short of true real-time operation; *iii)* the processor used in [34] can be easily upgraded to improve performance; we may conclude that real-time decoding is certainly possible. Regarding latency, in a CS system it is given by the length of the window (256 ms) plus the decoding time (smaller than 256 ms), so in the range 256-512 ms. Our control loop operates on the order of 1-2 s (matching the natural timescale of limb movement and stimulation adaptation), this latency is acceptable for integration in real-time CS.

### B. FES CONTROL

This section reports the experimental analysis and results related to the evaluation between the voluntary movements of the healthy arm (simulated by the dominant upper limb) and the stimulated movements replications performed by the paralyzed arm (simulated by the non-dominant upper limb). The first part of the analysis focused on the evaluation and comparison of movement parameters: height, velocity and angle. The amplitudes of the these parameters were normalized to those acquired from the set up phase. Then, to accurately capture the normalized parameters profiles over time, we first synchronized the cameras, ensuring reliable motion tracking despite the stimulated limb's inherent response latency. Next, we overlaid the voluntary and stimulated motion profiles to compare their progression over time.

For each subject and test session, both CoC and Cross-correlation metrics were calculated on the height, angle and velocity profiles of voluntary versus stimulated movements. These metrics help to quantitatively validate the approach after comparing it with the survey responses. In Fig. 7 an example is reported. It can be noted that test session 5 received the highest rating scores across nearly all measured variables, most notably for the Intensity variable (Fig. 7a). The survey responses align perfectly with CoC and Cross-correlation values calculated on the movement parameters across all test sessions. The highest CoC value (0.79001) was observed for the test session 5 as shown in the movement parameters profiles over time in Fig. 7b. On the other hand, the lowest CoC value (0.23451) was obtained during test session 3 (Fig. 7c).

The initial analysis reveals that there is at least one configuration among the tested combinations of $f_s$ and $PW$ stimulation parameters that is more functional and responsive than the others. Therefore, the FES control system can be effectively implemented into the existing framework, ensuring reliability and enabling automatic and dynamic management of stimulation effects. The implemented configuration protocol highlights the need to control for patient variability in voluntary effort, since patients cannot reproduce movements at a consistent intensity across all the repetitions. This variability directly affects the stimulation delivered to the affected limb. This variability arises from the lack of constraints on the healthy arm's voluntary movements to standardize the intensity over repetitions. While applying a constraint, such as lifting weights, could enhance the repeatability of contractions, the weight would have to vary for each subject based on their unique physiological muscle conditions. For this reason, it was decided to take into account the analysis of movements performed by both the healthy and paralyzed upper limb with the $AS_{ATC}$.

Fig. 8, illustrates three scenarios that can arise during the test session. In Fig. 8a, the height profiles of the healthy (blue) and paralyzed (dashed green) arms are overlaid with the $AS_{ATC}$ stimulation pulse (red), illustrating that, even with a correct delivered pulse waveform, the paralyzed arm movement remains minimal. This is an example of an ineffective configuration of FES parameters. The second case

in Fig. 8b, presents a normal $AS_{ATC}$ intensity pulse with a correct output movement of the paralyzed arm. This is the ideal response of the patient that should be obtained with an effective configuration of the stimulation parameters. The final scenario in Fig. 8c demonstrates the impact of varying the healthy limb's contraction intensity. Indeed, there is a minimal movement of the paralyzed arm due to a low intensity $AS_{ATC}$ stimulation contraction during the first repetition. On the other hand, the second repetition shows a normal $AS_{ATC}$ intensity while the stimulated arm response is almost nonexistent. This may be justified by the fact that the combination of stimulation parameters was not adequate for the specific subject.

The trial proves that there is a subjectivity related to the combination of stimulation parameters that differentiates the choice of one combination over another for the specific subject. In Fig. 9, a global analysis was carried out on the tested population, comparing the survey rating scores with the maximum cross-correlation values between healthy and stimulated limbs. Intensity was evaluated with high score (score = 4) for test session 1 and with medium high score (score = 3) for test sessions 3 and 5 by the largest part of tested population (Fig. 9a). The lowest score of the same variable was observed for test sessions 2 (score = 2) and 4 (score = 1). The same consideration can be performed on the scores given for the Easiness variable. Tests 1, 3 and 5 were perceived highly effective and at the same time the most easy to perform (score = 4). On the other hand, tests 2 and 4 received lower ratings indicating a less physiological performance (score = 1 and score = 2, respectively), as shown in Fig. 9d). Easiness and Intensity resulted as the most important variables to assess the effectiveness of test sessions FES configuration. The other variables were used as control parameters. Indeed, the major part of the population considered Pain, Annoyance and Fatigue in a score range between 1 and 2 (Fig. 9b, 9c, 9e). The percentage of subjects that found test sessions 1, 3 and 5 as the more physiological and intense ones align with the 3 highest maximum Cross-correlation values calculated on the angle parameters (Fig. 9f). For each test session, the mean of the peak Cross-correlation values across all subjects is reported.

Notably, 22% of participants rated test session 1 as the more intense, indicating a stronger correlation between healthy and paralyzed movements. Tests 3 and 5 garnered a similar rating from 28% of participants. By contrast, tests 2 and 4 were considered least effective with the 9% and 13%, respectively. The lowest Cross-correlation values identify a test session configuration which was not effective.

The test results identified the stimulation parameters that most effectively maximized motion performance in accordance with each subject's perceived sensation. Indeed, the stimulation configurations that yielded the strongest

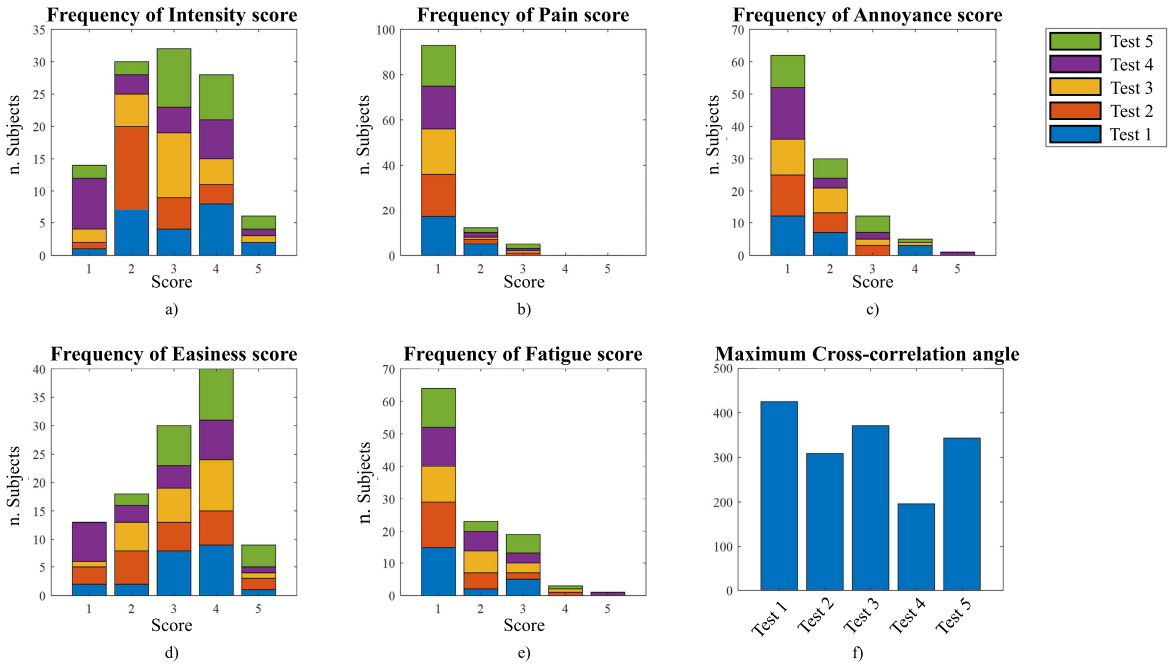


**FIGURE 9.** a) to e) Survey answers given by all the subjects for the five test sessions. Each graph represents a variable. For each of them, each test session was evaluated in a score range from 1 to 5 (x axis). For each combination, the response frequency is shown (y axis). f) The mean maximum value of cross-correlation above all the subjects between healthy and paralyzed arms movements. a) Intensity was largely evaluated with high score (score = 4) for test session 1 and with medium high score (score = 3) for test sessions 3 and 5. The lowest score was rated for test sessions 2 (score = 2) and 4 (score = 1). d) Scores given for Easiness indicate that tests 1, 3 and 5 were felt highly effective by the majority and at the same time the most easy to perform (score = 4). On the other hand, tests 2 and 4 received lower scores meaning a less physiological performance (score = 1 and score = 2, respectively). b), c), e) The major part of the population considered Pain, Annoyance and Fatigue in a score range between 1 and 2. f) The 3 highest maximum value evaluated on the cross-correlations of the angles matches with the percentage of the subjects that found as more physiological and intense test sessions 1, 3 and 5.

responses, both in terms of affected limb movement and perceived sensation, also most closely matched the parameters generated by the real-time loop-control system tested in parallel. The obtained results demonstrate the concrete possibility of meeting the clinical need of long-term control therapy with motion tracking. The correlation values obtained and the performance of the control system by comparing its optimal stimulation parameters with the responses of the subjects to each tested configuration show that the tested FES control allows for automatized processes, with a patient based setting of pulse parameters.

This finding lead to greater effectiveness of the treatment and reduce the need for manual intervention. Based on the obtained results, we can state that the proposed system enables precise, personalized and automated stimulation for each specific patient, providing synchronized movement data during performance. Additionally, our contributions specifically address critical barriers to widespread adoption of FES systems in real-world settings. By minimizing hardware complexity and overall cost, the proposed platform promotes accessibility and scalability across diverse healthcare environments, including under-resourced or decentralized facilities. The streamlined setup process and intuitive, automatic parameter adjustment relieve the burden on therapists, enhancing usability and reducing reliance on specialized operator training. Unlike traditional manual tuning approaches, our system enables consistent and reproducible stimulation protocols through real-time quantitative control. Furthermore, the integration of remote operability and feedback mechanisms lays the foundation for tele-rehabilitation applications—an essential consideration in contexts where frequent in-person therapy is logistically or economically unfeasible. We highlight that these results do not aim to evaluate therapeutic outcomes or to statistically validate the efficacy of stimulation protocols in a clinical population. The current work focuses on healthy subjects and serves as a proof-of-concept for the closed-loop stimulation control and the system-level performance.

This preliminary validation step with healthy subjects serve as a basis for the future authorization to initiate a clinical trial involving post-stroke patient for the evaluation of the actual therapeutic efficacy of the system which has not yet received CE certification. This procedure is in line with standard development pathways for medical devices according to the European Medical Device Regulation 2017/745 (MDR). This current work was specifically designed to demonstrate technical feasibility, system reliability, and user safety, all of which are essential prerequisites before seeking clinical-grade certification and patient trials.

Clinical trials of FES in acute stroke report that approximately 60-75% of patients experience significant improvements in reaching and grasping function [35], and a recent investigation observed meaningful motor control gains in 65% of participants using adaptive stimulation protocols [36]. In this population, several factors, spastic hypertonia, sensory and proprioceptive deficits, high inter-patient variability in lesion characteristics, muscle fatigue susceptibility, and challenges in electrode contact quality, can impact both comfort and movement efficacy [35], [36]. Although this study was conducted in healthy volunteers, future work will be based on clinical trials involving post-stoke survivors, as system validation.

To further enhance the characterization of the motion control loop, we plan to investigate the relevance of additional features such as velocity profiles, acceleration peaks, jerk metrics, and fatigue indices. These feedback parameters are expected to play a more significant role in the context of more complex movements, which are planned as part of our future work.

### C. MUSCLE FATIGUE

Electrical stimulated muscle contractions impact fatigue differently compared to voluntary contractions. The fiber recruitment in voluntary contractions follows Henneman's principle [37]: type I fibers (less fatigable but producing weaker tensive force) activate first, followed by type II fibers (more fatigable but producing stronger contractions). On the other hand, in stimulated contraction fiber recruitment is non-physiological and random, depending on which fibers are in the electrodes path [38]. This affects the recruitment frequency, which is higher during stimulated contractions, consequently leading to a different impact on muscle fatigue [39]. In natural conditions, the central nervous system mitigates muscle fatigue by alternately recruiting new motor units and resting fatigued ones. Simple bipolar electrical stimulation, however, cannot replicate this adaptive mechanism, as it only stimulates fibers along the current pathway. To better mimic physiological recruitment, advanced techniques like distributed stimulation are employed [40].

FES-stimulated contractions can increase muscle fatigue but offer an advantage for maintaining or improving muscle mass. By recruiting in random order, type II fibers are also activated, which are physiologically engaged only during high-intensity efforts that bedridden patients cannot perform.

During the fatigue test conducted in this study each subject repeated arm flex-extension 20 times using the parameters from test session 1. The fatigue assessment was included to determine how many exercise repetitions a specific patient can perform while maintaining maximal stimulation efficiency relative to the performed movement. In fact, statistically, most participants reported feeling fatigue towards the end of the session, at time points 4 and 5 (i.e. between 12 and 20 repetitions), referring to Fig.10. Furthermore, identifying muscle fatigue is crucial to distinguish it from an ineffective stimulation when the stimulated limb cannot fully perform the movement.

To this end, we utilized the motion-tracking system to evaluate movement performance from one repetition to the next, since a gold standard EMG-based implementation is inconclusive in this context. Indeed, the sEMG signal would be distorted by the electrical stimulation itself, yielding misleading information about actual muscle activity.

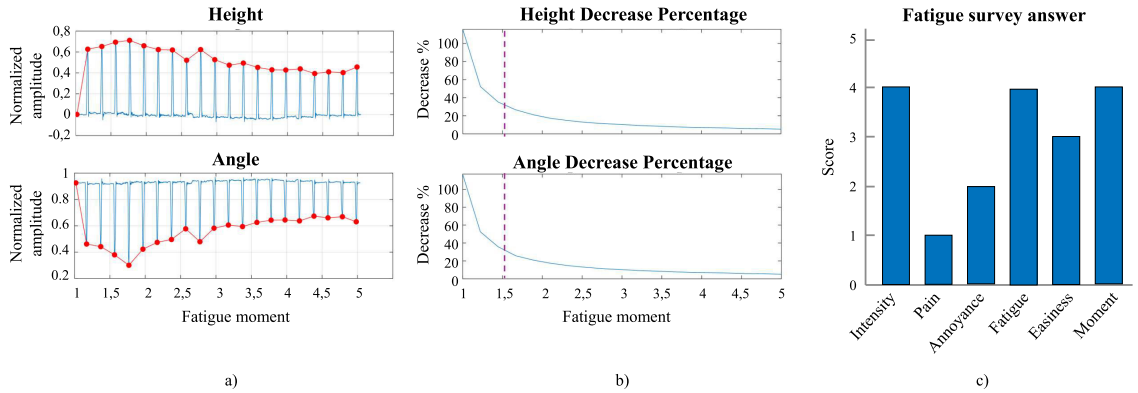


**FIGURE 10.** Example of a subject fatigue profile. a) Time-series of height and angle parameters across repetitions, with peak values beginning to decrease after the first 10 repetitions. b) Percentage of decrease between peaks for each variable during the moment of test session between 1 to 5. c) Survey responses given by the subject: both Intensity and Fatigue score are rated as 4. "Moment = 1" denotes that fatigue was reported at the very start of the session.

In addition to assessing movement parameters of height and angle across repetitions, the study also included a subject reported perceived fatigue index in the administered survey.

Furthermore, in the survey, most participants reported low Fatigue levels, although a relevant percentage rated it as a 4 over 5, while Pain and Discomfort were rated as minimal ensuring test safety. The fatigue profile resulted similar among all subjects. An example is illustrated in Fig. 10, where the decreasing peaks related to height and angle measurements during repetition are noticeable (Fig. 10a). Notably, the survey responses (Fig. 10c) related to the moment in which participants first felt fatigue during the session (score = 1), align with the point on the curve where the peaks start decreasing (1.5). These results are related to healthy participants and, consequently, it is likely that fatigue effect would be more pronounced in hemiplegic subjects than in healthy ones.

Compared to previous FES control studies, reported in Table 1, our system achieves competitive performance in terms of trajectory replication, with a maximum CoC of 0.79 between healthy and impaired limbs. Unlike previous works, which either apply fixed stimulation parameters [12], [16], [17] or rely on non-motor feedback such as EMG signals [13], [14], our method implements a real-time closed-loop control strategy. Specifically, stimulation parameters are dynamically adapted based on trajectory error, enabling more accurate and responsive rehabilitation compared to fixed-profile or threshold-based controllers.

## VI. CONCLUSION

This study presents the experimental results obtained with an enhanced FES control system, designed to automatically adjust stimulation pulse parameters ($f_s$ and $PW$) for each patient in a precise and controlled way. The proof-of-concept results demonstrate the system's potential to enable automatic and real-time control of FES pulse settings, which are typically selected manually by the operator, going beyond the latest work on FES control system [9]. As shown, for each subject exists at least one parameters configuration, corresponding to one that the feedback control loop would have reached, that allows for better motion performance. Additionally, this approach, combined with MT, may enhances rehabilitation effectiveness by facilitating more controlled and responsive stimulation. All the control loop has a high reproducibility, requiring only two additional cameras for the movement tracking. Moreover, the integration of the CS block, allows the operators to keep track of the sEMG signal in a reliable way, which, to date, is not yet present in the current state of art. Future improvements may involve incorporating data-driven techniques to optimize pulse parameters selection. Overall, the presented testing trial demonstrates that the proposed system wants to be a valid and practical solution for automated and controlled FES in rehabilitation field.

**TABLE 2.** List of acronyms.

| Acronym | Definition |
|---|---|
| FES | Functional Electrical Stimulation |
| MT | Mirror Therapy |
| sEMG | Surface Electromyography |
| CS | Compressed Sensing |
| MT | Mirror Therapy |
| GUI | Graphical User Interface |
| PW | Pulse Width |
| fs | Stimulation Frequency |
| ATC | Average Threshold Crossing |
| CR | Compression Ratio |
| RMS | Root Mean Square |
| CE | European Conformity |
| MDR | Medical Device Regulation |
| IEC | International Electrotechnical Commission |
| CoC | Correlation Coefficient |
| AS | Activation Signal |
| BLE | Bluetooth Low Energy |
| AFEs | Multiple Analog Front Ends |
| TC | Threshold Crossing |
| MCU | Micro Controller Unit |

## REFERENCES


[1] D. B. Gandhi, A. Sterba, H. Khatter, and J. D. Pandian, "Mirror therapy in stroke rehabilitation: Current perspectives," *Therapeutics Clin. Risk Manage.*, pp. 75–85, Feb. 2020, doi: 10.2147/tcrm.s206883.

[2] R. Palomo-Carrión, J. C. Zuil-Escobar, M. Cabrera-Guerra, P. Barreda-Martínez, and C. B. Martínez-Cepa, "Mirror therapy and action observation therapy to increase the affected upper limb functionality in children with hemiplegia: A randomized controlled trial protocol," *Int. J. Environ. Res. Public Health*, vol. 18, no. 3, p. 1051, Jan. 2021, doi: 10.3390/ijerph18031051.

[3] A. W. Azman, J. Naeem, and Y. M. Mustafah, "The design of non-invasive functional electrical stimulation (FES) for restoration of muscle function," in *Proc. Int. Conf. Comput. Commun. Eng. (ICCCE)*, Jul. 2012, pp. 612–616, doi: 10.1109/ICCCE.2012.6271260.

[4] D. Bhatia, G. Bansal, R. P. Tewari, and K. K. Shukla, "State of art: Functional electrical stimulation (FES)," *Int. J. Biomed. Eng. Technol.*, vol. 5, no. 1, pp. 77–99, 2011, doi: 10.1504/ijbet.2011.038474.

[5] C. M. Niu, Y. Bao, C. Zhuang, S. Li, T. Wang, L. Cui, Q. Xie, and N. Lan, "Synergy-based FES for post-stroke rehabilitation of upper-limb motor functions," *IEEE Trans. Neural Syst. Rehabil. Eng.*, vol. 27, no. 2, pp. 256–264, Feb. 2019.

[6] L. G. Moseley, A. Gallace, and C. Spence, "Is mirror therapy all it is cracked up to be? Current evidence and future directions," *Pain*, vol. 138, no. 1, pp. 7–10, Aug. 2008, doi: 10.1016/j.pain.2008.06.026.

[7] H. Kim, G. Lee, and C. Song, "Effect of functional electrical stimulation with mirror therapy on upper extremity motor function in poststroke patients," *J. Stroke Cerebrovascular Diseases*, vol. 23, no. 4, pp. 655–661, Apr. 2014, doi: 10.1016/j.jstrokecerebrovasdis.2013.06.017.

[8] S. Mathieson, J. Parsons, and M. S. Kaplan, "Combining functional electrical stimulation with mirror therapy for the upper limb in people with stroke," *Crit. Rev. Phys. Rehabil. Med.*, vol. 26, nos. 1–2, pp. 113–129, 2014.

[9] A. Prestia, F. Rossi, A. Mongardi, P. M. Ros, M. R. Roch, M. Martina, and D. Demarchi, "Motion analysis for experimental evaluation of an event-driven FES system," *IEEE Trans. Biomed. Circuits Syst.*, vol. 16, no. 1, pp. 3–14, Feb. 2022, doi: 10.1109/TBCAS.2021.3137027.

[10] F. Rossi, A. Mongardi, P. M. Ros, M. R. Roch, M. Martina, and D. Demarchi, "Tutorial: A versatile bio-inspired system for processing and transmission of muscular information," *IEEE Sensors J.*, vol. 21, no. 20, pp. 22285–22303, Oct. 2021, doi: 10.1109/JSEN.2021.3103608.

[11] M. R. Popovic, K. Masani, and S. Micera, "Functional electrical stimulation therapy: Recovery of function following spinal cord injury and stroke," in *Neurorehabilitation Technology*. London, U.K.: Springer, 2016, pp. 513–532, doi: 10.1007/978-1-4471-2277-7_7.

[12] D. Wolf, N. Dunkelberger, C. G. McDonald, K. Rudy, C. Beck, M. K. O'Malley, and E. Schearer, "Combining functional electrical stimulation and a powered exoskeleton to control elbow flexion," in *Proc. Int. Symp. Wearable Robot. Rehabil. (WeRob)*, Nov. 2017, pp. 1–2, doi: 10.1109/WEROB.2017.8383860.

[13] Y.-X. Zhou, H.-P. Wang, X.-P. Cao, Z.-Y. Bi, Y.-J. Gao, X.-B. Chen, X.-Y. Lü, and Z.-G. Wang, "Electromyographic bridge—A multi-movement volitional control method for functional electrical stimulation: Prototype system design and experimental validation," in *Proc. 39th Annu. Int. Conf. IEEE Eng. Med. Biol. Soc. (EMBC)*, Jul. 2017, pp. 205–208, doi: 10.1109/EMBC.2017.8036798.

[14] Z.-Y. Bi, X.-L. Bao, H.-P. Wang, X.-Y. Lv, and Z.-G. Wang, "Prototype system design and experimental validation of gait-oriented EMG bridge for volitional motion function rebuilding of paralyzed leg," in *Proc. IEEE 7th Int. Conf. Bioinf. Comput. Biol. (ICBCB)*, Mar. 2019, pp. 79–82, doi: 10.1109/ICBCB.2019.8854632.

[15] Z. Bi, Y. Wang, H. Wang, Y. Zhou, C. Xie, L. Zhu, H. Wang, B. Wang, J. Huang, X. Lu, and Z. Wang, "Wearable EMG bridge—A multiple-gesture reconstruction system using electrical stimulation controlled by the volitional surface electromyogram of a healthy forearm," *IEEE Access*, vol. 8, pp. 137330–137341, 2020, doi: 10.1109/ACCESS.2020.3011710.

[16] S. Carvalho, A. Correia, J. Figueiredo, J. M. Martins, and C. P. Santos, "Functional electrical stimulation system for drop foot correction using a dynamic NARX neural network," *Machines*, vol. 9, no. 11, p. 253, Oct. 2021, doi: 10.3390/machines9110253.

[17] Y. Li, X. Yang, Y. Zhou, J. Chen, M. Du, and Y. Yang, "Adaptive stimulation profiles modulation for foot drop correction using functional electrical stimulation: A proof of concept study," *IEEE J. Biomed. Health Informat.*, vol. 25, no. 1, pp. 59–68, Jan. 2021, doi: 10.1109/JBHI.2020.2989747.

[18] J. Secco, "Methodology for telerehabilitation with active tracking methodology of results and in real time," IT Patent 102 024 000 026 373, Nov. 22, 2024.

[19] D. Maji, S. Nagori, M. Mathew, and D. Poddar, "YOLO-pose: Enhancing YOLO for multi person pose estimation using object keypoint similarity loss," in *Proc. IEEE/CVF Conf. Comput. Vis. Pattern Recognit. Workshops (CVPRW)*, Jun. 2022, pp. 2636–2645.

[20] J. Secco, M. Poggio, and F. Corinto, "Supervised neural networks with memristor binary synapses," *Int. J. Circuit Theory Appl.*, vol. 46, no. 1, pp. 221–233, Jan. 2018, doi: 10.1002/cta.2429.

[21] Y. S. Kim, S. H. Shin, J. Secco, K. S. Min, and F. Corinto, "Memristor-based platforms: A comparison between continous-time and discrete-time cellular neural networks," in *Advances in Neuromorphic Hardware Exploiting Emerging Nanoscale Device*. New Delhi, India: Springer, 2017, pp. 65–79, doi: 10.1007/978-81-322-3703-7_4.

[22] Ultralytics. (2024). *Pose-Ultralytics YOLO*. [Online]. Available: https://docs.ultralytics.com/it/tasks/pose/#models

[23] F. Wang, G. Wang, and B. Lu, "YOLOv8-PoseBoost: Advancements in multimodal robot pose keypoint detection," *Electronics*, vol. 13, no. 6, p. 1046, 2024.

[24] D. L. Donoho, "Compressed sensing," *IEEE Trans. Inf. Theory*, vol. 52, no. 4, pp. 1289–1306, Apr. 2006, doi: 10.1109/TIT.2006.871582.

[25] R. Baraniuk, M. Davenport, R. DeVore, and M. Wakin, "A simple proof of the restricted isometry property for random matrices," *Constructive Approximation*, vol. 28, no. 3, pp. 253–263, Dec. 2008, doi: 10.1007/s00365-007-9003-x.

[26] M. Mangia, F. Pareschi, R. Rovatti, and G. Setti, "Implicit notch filtering in compressed sensing by spectral shaping of sensing matrix," in *Proc. IEEE Int. Symp. Circuits Syst. (ISCAS)*, May 2016, pp. 257–260, doi: 10.1109/ISCAS.2016.7527219.

[27] F. Pareschi, P. Albertini, G. Frattini, M. Mangia, R. Rovatti, and G. Setti, "Hardware-algorithms co-design and implementation of an analog-to-information converter for biosignals based on compressed sensing," *IEEE Trans. Biomed. Circuits Syst.*, vol. 10, no. 1, pp. 149–162, Feb. 2016, doi: 10.1109/TBCAS.2015.2444276.

[28] L. Zhang, J. Chen, C. Ma, X. Liu, and L. Xu, "Performance analysis of electromyogram signal compression sampling in a wireless body area network," *Micromachines*, vol. 13, no. 10, p. 1748, Oct. 2022.

[29] J. Haboba, M. Mangia, F. Pareschi, R. Rovatti, and G. Setti, "A pragmatic look at some compressive sensing architectures with saturation and quantization," *IEEE J. Emerg. Sel. Topics Circuits Syst.*, vol. 2, no. 3, pp. 443–459, Sep. 2012, doi: 10.1109/JETCAS.2012.2220392.

[30] D. A. Winter, "Frontmatter," in *Biomechanics and Motor Control of Human Movement*. Hoboken, NJ, USA: Wiley, 2009, doi: 10.1002/9780470549148.fmatter.

[31] H. Choi, D. Park, D.-W. Rha, H. S. Nam, Y. J. Jo, and D. Y. Kim, "Kinematic analysis of movement patterns during a reach-and-grasp task in stroke patients," *Frontiers Neurol.*, vol. 14, Aug. 2023, Art. no. 1225425, doi: 10.3389/fneur.2023.1225425.

[32] K.-C. Lin, P.-C. Huang, Y.-T. Chen, C.-Y. Wu, and W.-L. Huang, "Combining afferent stimulation and mirror therapy for rehabilitating motor function, motor control, ambulation, and daily functions after stroke," *Neurorehabilitation Neural Repair*, vol. 28, no. 2, pp. 153–162, Feb. 2014.

[33] W. Zeng, Y. Guo, G. Wu, X. Liu, and Q. Fang, "Mirror therapy for motor function of the upper extremity in patients with stroke: A meta-analysis," *J. Rehabil. Med.*, vol. 50, no. 1, pp. 8–15, 2018.

[34] F. Pareschi, M. Mangia, D. Bortolotti, A. Bartolini, L. Benini, R. Rovatti, and G. Setti, "Energy analysis of decoders for rakeness-based compressed sensing of ECG signals," *IEEE Trans. Biomed. Circuits Syst.*, vol. 11, no. 6, pp. 1278–1289, Dec. 2017, doi: 10.1109/TBCAS.2017.2740059.

[35] T. A. Thrasher, V. Zivanovic, W. McIlroy, and M. R. Popovic, "Rehabilitation of reaching and grasping function in severe hemiplegic patients using functional electrical stimulation therapy," *Neurorehabilitation Neural Repair*, vol. 22, no. 6, pp. 706–714, Nov. 2008, doi: 10.1177/1545968308317436.

[36] M. A. Khan, H. Fares, H. Ghayvat, I. C. Brunner, S. Puthusserypady, B. Razavi, M. Lansberg, A. Poon, and K. J. Meador, "A systematic review on functional electrical stimulation based rehabilitation systems for upper limb post-stroke recovery," *Frontiers Neurol.*, vol. 14, Dec. 2023, Art. no. 1272992, doi: 10.3389/fneur.2023.1272992.

[37] E. Henneman and C. B. Olson, "Relations between structure and function in the design of skeletal muscles," *J. Neurophysiol.*, vol. 28, no. 3, pp. 581–598, May 1965, doi: 10.1152/jn.1965.28.3.581.

[38] C. L. Lynch and M. R. Popovic, "Functional electrical stimulation," *IEEE Control Syst. Mag.*, vol. 28, no. 2, pp. 40–50, Feb. 2008, doi: 10.1109/MCS.2007.914689.
[39] T. Kesar and S. Binder-Macleod, "Effect of frequency and pulse duration on human muscle fatigue during repetitive electrical stimulation," *Experim. Physiol.*, vol. 91, no. 6, pp. 967–976, Nov. 2006, doi: 10.1113/expphysiol.2006.033886.
[40] A. J. Buckmire, D. R. Lockwood, C. J. Doane, and A. J. Fuglevand, "Distributed stimulation increases force elicited with functional electrical stimulation," *J. Neural Eng.*, vol. 15, no. 2, Apr. 2018, Art. no. 026001, doi: 10.1088/1741-2552/aa9820.

**ELISABETTA SPINAZZOLA** (Graduate Student Member, IEEE) received the bachelor's degree in medical system engineering and the master's degree in biomedical engineering from Politecnico di Torino, Turin, Italy, in 2020 and 2022, respectively, where she is currently pursuing the Ph.D. degree with the Department of Electronics and Telecommunications. From June to November 2022, she worked an Internship Program with Elitech Group S.r.l. Company. From November 2022 to October 2023, she was a Research Fellow with the Molecular Biotechnology Center, Università di Torino, as a Software Developer. From November 2023 to October 2024, she continued as a Research Fellow with the Department of Electronics and Telecommunications, Politecnico di Torino. Her research interests include the elaboration and development of biomedical system applications, as well as signal and image processing, mainly focusing on the rehabilitation field, wound care, and monitoring wearable device.

**ANDREA MONGARDI** (Member, IEEE) received the bachelor's and master's degrees in electronic engineering, embedded systems specialization from Politecnico di Torino, Turin, Italy, in 2017 and 2019, respectively, where he is currently pursuing the Ph.D. degree with the Department of Electronics and Telecommunications, focusing on the design of low power embedded systems for sEMG acquisition. He is a member of the Micro and Nano Electronic Systems (MiNES) Laboratory.

**FABIO ROSSI** (Member, IEEE) received the M.Sc. degree in biomedical engineering and the Ph.D. degree in electronic engineering from Politecnico di Torino, Turin, Italy, in 2017 and 2022, respectively. Since 2016, he has been a Research Member of the Micro and Nano Electronic System (MiNES) Group, Department of Electronics and Telecommunications (DET), Politecnico di Torino. His research interests include the design of low-power sEMG acquisition and processing networks for healthcare monitoring systems, rehabilitative applications, and human–machine interfaces.

**ANDREA PRESTIA** (Member, IEEE) received the bachelor's and master's degrees in biomedical engineering from Politecnico di Torino, Turin, Italy, in 2018 and 2020, respectively, where he is currently pursuing the Ph.D. degree with the Department of Electronics and Telecommunications. He is a member of the Micro and Nano Electronic System (MiNES) Research Group. His research interests include the design and development of electronic systems for biomedical applications, mainly focusing on the rehabilitation field.

**SARA BECCHI** received the bachelor's and master's degrees in biomedical engineering from Politecnico di Torino, in 2022 and 2024, respectively, specializing in biomedical instrumentation. She is currently a Research Fellow with Politecnico di Torino. Her research interests include electronics applied to biomedical engineering, particularly in the fields of rehabilitation, signal analysis, and both real-time and offline image analysis.

**ROSANNA CAVAZZANA** received the bachelor's degree in biomedical engineering and the M.S. degree in e-Health from Politecnico di Torino, Italy, in 2023 and 2024, respectively, where she is currently pursuing the Ph.D. degree in electronic with the Department of Electronic and Telecommunications. Her research interests include data analysis and deep learning models with applications in the biomedical field.

**FEDERICA SAVI** received the bachelor's degree in physiotherapy from the University of Parma, in 2015, and the master's degree in rehabilitation sciences of health professions from the University of Florence. She is currently a Physiotherapist with Fondazione Don Carlo Gnocchi Onlus, Parma.

**JACOPO SECCO** received the bachelor's and master's degrees in biomedical engineering, and the Ph.D. degree in electronic engineering from Politecnico di Torino, in 2012 and 2013, respectively, focusing on memristive neural networks and neuromorphic systems. In 2015, he co-founded Omnidermal Biomedics. He is currently an Assistant Professor with Politecnico di Torino. He is an Engineer and an Entrepreneur specializing in biomedical engineering and neuromorphic systems. His work focuses on developing simplified models of memristors and neuromorphic components for AI circuits, contributing to the advancement of next-generation computing technologies. His research interests include memristor-based circuits, neuromorphic engineering, and artificial intelligence for biomedical applications.

**DANILO DEMARCHI** (Senior Member, IEEE) received the Engineering and Ph.D. degrees in electronics engineering from Politecnico di Torino, Turin, Italy, in 1991 and 1995, respectively. He is currently a Full Professor with the Department of Electronics and Telecommunications, Politecnico di Torino. He was a Visiting Professor with Tel Aviv University, Tel Aviv, Israel, from 2018 to 2021, and EPFL, Lausanne, in 2019. He was a Visiting Scientist with Massachusetts Institute of Technology and Harvard Medical School, in 2018. He is the author and co-author of five patents and more than 300 international scientific publications. He is the Leader of the Micro and Nano Electronic Systems (MiNES) Laboratory, Politecnico di Torino. He is a member of the IEEE Sensors Council and the IEEE BioCAS Technical Committee, the General Chair of IEEE BioCAS 2017, and a Founder of the IEEE FoodCAS Workshop (Circuits and Systems for Better Quality Food). He is an Associate Editor for IEEE Sensors Journal, IEEE Open Journal of Engineering in Medicine and Biology, and *BioNanoScience* journal (Springer).

**FABIO PARESCHI** (Senior Member, IEEE) received the Dr.Eng. degree (Hons.) in electronic engineering from the University of Ferrara, Ferrara, Italy, in 2001, and the Ph.D. degree in information technology from the University of Bologna, Bologna, Italy, in 2007, under the European Doctorate Project (EDITH). He is currently an Associate Professor with the Department of Electronic and Telecommunication, Politecnico di Torino. He is also a Faculty Member with ARCES, University of Bologna. His research interests include analog and mixed-mode electronic circuit design, statistical signal processing, compressed sensing, dc-dc converters, random number generation and testing, and electromagnetic compatibility. He was a recipient of the 2019 IEEE BioCAS Transactions Best Paper Award, the Best Paper Award at ECCTD 2005, and the Best Student Paper Award at EMC Zurich 2005 and IEEE EMCCompo 2019. From 2010 to 2013, he was an Associate Editor for IEEE Transactions on Circuits and Systems II: Express Briefs and IEEE Open Journal of Circuits and Systems, from 2020 to 2022.

**GIANLUCA SETTI** (Fellow, IEEE) received the Dr.Eng. (Hons.) and Ph.D. degrees in electronic engineering from the University of Bologna, in 1992 and 1997, respectively. From 1997 to 2017, he was with the Department of Engineering, University of Ferrara, Italy, as an Assistant, from 1998 to 2000, an Associate, from 2001 to 2008, and as a Professor, from 2009 to 2017, of circuit theory and analog electronics. From 2017 to 2022, he was a Professor of electronics, signal, and data processing with the Department of Electronics and Telecommunications (DET), Politecnico di Torino, Italy. Since November 2022, he has been the Dean of the Computer, Electrical, Mathematical Sciences and Engineering (CEMSE) Division and a Professor of electrical and computer engineering (ECE) program with the King Abdullah University of Science and Technology (KAUST), Saudi Arabia. He held several positions as a Visiting Professor/a Scientist with EPFL, in 2002 and 2005, UCSD, in 2004, IBM, in 2004 and 2007, and the University of Washington, in 2008 and 2010. His research interests include nonlinear circuits, recurrent neural networks, electromagnetic compatibility, compressive sensing and statistical signal processing, biomedical circuits and systems, power electronics, design and implementation of IoT nodes, circuits and systems for machine learning, and applications of AI techniques for anomaly detection and predictive maintenance He was a Distinguished Lecturer of the IEEE CAS Society, from 2004 to 2005 and from 2013 to 2014, a member of the CASS Board of Governors, from 2005 to 2008, of the same Society, and served as the 2010 CAS Society President. He received the 2013 IEEE CAS Society Meritorious Service Award. He was a co-recipient of the 2004 IEEE CAS Society Darlington Award, the 2013 IEEE CAS Society Guillemin-Cauer Award, the 2019 IEEE Transactions on Circuits and Systems Best Paper Award, and the Best Paper Award at ECCTD2005, and the Best Student Paper Award at EMCZurich2005 and ISCAS2011. He also received the 1998 Caianiello Prize for the Best Italian Ph.D. Thesis on Neural Networks. He served as an Associate Editor for IEEE Transactions on Circuits and Systems—Part I, from 1999 to 2002 and from 2002 to 2004, and IEEE Transactions on Circuits and Systems—Part II, from 2004 to 2007, the Deputy-Editor-in-Chief for *IEEE Circuits and Systems Magazine*, from 2004 to 2007, the Editor-in-Chief for IEEE Transactions on Circuits and Systems—Part II, from 2006 to 2007, and IEEE Transactions on Circuits and Systems—Part I, from 2008 to 2009. He also served in the Editorial Board of IEEE Access, from 2013 to 2015, and *Proceedings of the IEEE*, from 2015 to 2018. In 2012, he was the Chair of the IEEE Strategic Planning Committee of the Publication Services and Products Board (PSPB-SPC). He was the first non-North-American Vice President of the IEEE for Publication Services and Products, in 2013 and 2014. He served in the program committee of many conferences and was, in particular, the Special Sessions Co-Chair of ISCAS2005 (Kobe) and ISCAS2006 (Kos), the Technical Program Co-Chair of NDES2000 (Catania), ISCAS2007 (New Orleans), ISCAS2008 (Seattle), ICECS2012 (Seville), BioCAS2013 (Rotterdam), and MWSCAS2023 (Phoenix), and the General Co-Chair of NOLTA2006 (Bologna) and ISCAS2018 (Florence). He is the Co-Editor of the book *Chaotic Electronics in Telecommunications* (CRC Press), Boca Raton, in 2000, *Circuits and Systems for Future Generation of Wireless Communications* (Springer), in 2009, and *Design and Analysis of Biomolecular Circuits* (Springer), in 2011, the Co-Author of the book *Adapted Compressed Sensing for Effective Hardware Implementations*, in 2018, and one of the guest editors of the May 2002 Special Issue of *Proceedings of the IEEE* on "Applications of Non-Linear Dynamics to Electronic and Information Engineering." From 2019 to 2024, he served for two terms as the first non U.S. Editor-in-Chief of *Proceedings of the IEEE*, the flagship journal of the Institute.